Ultrasonics 73 (2017) 49–66

Contents lists available at ScienceDirect

Ultrasonics

journal homepage: www.elsevier.com/locate/ultras

Dynamics of ultrasonic additive manufacturing

Adam Hehr, Marcelo J. Dapino *

Center for Ultrasonic Additive Manufacturing, NSF I/UCRC on Smart Vehicle Concepts, Department of Mechanical and Aerospace Engineering, The Ohio State University, 201 W 19th Ave., Columbus, OH 43210, United States

ARTICLE INFO

Article history:
Received 18 February 2016
Received in revised form 22 June 2016
Accepted 14 August 2016
Available online 17 August 2016

Keywords:
A. Ultrasonic additive manufacturing (UAM)
B. Ultrasonic welding
C. LTI modeling
D. Frequency response function (FRF) estimation
E. Piezoelectrics
F. In-situ measurements

ABSTRACT

Ultrasonic additive manufacturing (UAM) is a solid-state technology for joining similar and dissimilar metal foils near room temperature by scrubbing them together with ultrasonic vibrations under pressure. Structural dynamics of the welding assembly and work piece influence how energy is transferred during the process and ultimately, part quality. To understand the effect of structural dynamics during UAM, a linear time-invariant model is proposed to relate the inputs of shear force and electric current to resultant welder velocity and voltage. Measured frequency response and operating performance of the welder under no load is used to identify model parameters. Using this model and in-situ measurements, shear force and welder efficiency are estimated to be near 2000 N and 80% when welding Al 6061-H18 weld foil, respectively. Shear force and welder efficiency have never been estimated before in UAM. The influence of processing conditions, i.e., welder amplitude, normal force, and weld speed, on shear force and welder efficiency are investigated. Welder velocity was found to strongly influence the shear force magnitude and efficiency while normal force and weld speed showed little to no influence. The proposed model is used to describe high frequency harmonic content in the velocity response of the welder during welding operations and coupling of the UAM build with the welder.

© 2016 Elsevier B.V. All rights reserved.

1. Introduction

Ultrasonic additive manufacturing (UAM) or ultrasonic consolidation is a continuous solid-state additive manufacturing process where thin foils of similar or dissimilar metals are ultrasonically welded together in a layer by layer process to form gapless, 3D metal parts [1,2]. The process begins by bringing a tool piece called the sonotrode or horn into contact with a metallic foil under a controlled pressure or normal load. The foil is then joined to the pre-deposited metal beneath via high power ultrasonic vibrations. The circular design of the sonotrode allows it to rotate at a prescribed linear speed simultaneous to welding foil. Periodic CNC machining is utilized intermittent of welding to create complex internal features, machine cavities for embedding objects into the structure, and for net shaping welded components. The process has been improved upon by actuating the sonotrode with two high power piezoelectric transducers [3]. This dual actuation increases the delivered weld power from 1 kW in first generation systems to 9 kW. The increase in weld power greatly improves bond quality and enables the joining of stronger and stiffer materials. The sonotrode and high power piezoelectric transducer(s) are designed to resonate longitudinally near 20 kHz. A schematic of the UAM process is shown in Fig. 1 and a commercial 9 kW UAM system is shown in Fig. 2.

The key mechanisms for ultrasonic metal welding include oxide fracture under pressure and plastic deformation of surface asperities through shear [4–6]. Oxide dispersal allows nascent metal surfaces to come into contact and form metallic bonds while surface asperity deformation promotes dynamic recrystallization of the interface microstructure [7–10]. The result is a narrow weld region on the order of 10–20 μm in size and bulk temperatures far below metallic melting temperatures [11]. Consequently, dissimilar metals can be welded together with minimal intermetallic formation [12–16], metallurgical changes are minimized and highly localized to the interface region, and temperature sensitive metals or components can be combined or built into metal structures [17–21].

The aim of this paper is to describe UAM system dynamics and power conversion within the welder using a linear time-invariant (LTI) model which explicitly specifies welder shear force and electric current as system inputs. The outputs of the model are welder velocity and electric voltage. The model describes the conversion and transfer of electrical to mechanical power within the welder. The model does not directly describe energy transferred to the weld, although it can be used as part of a broader modeling framework to quantify the complete flow of energy through the welder

* Corresponding author.
E-mail address: dapino.1@osu.edu (M.J. Dapino).

http://dx.doi.org/10.1016/j.ultras.2016.08.009
0041-624X/© 2016 Elsevier B.V. All rights reserved.

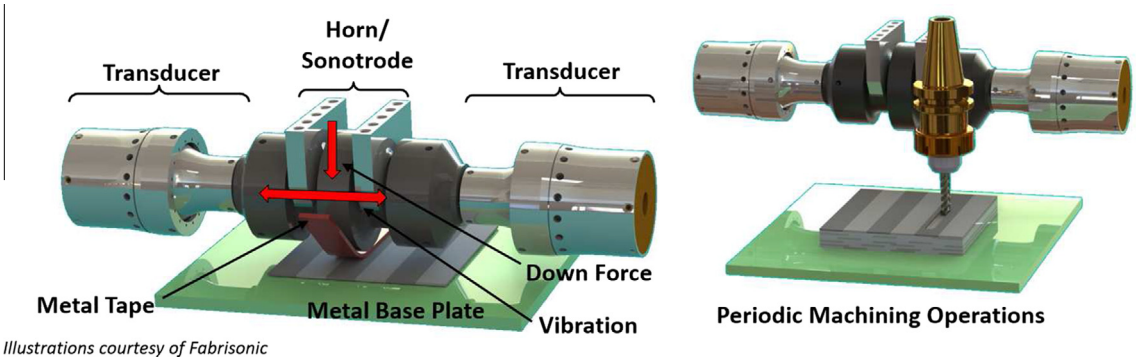

Fig. 1. Schematic representation of a 9 kW ultrasonic additive manufacturing welder (left) and the subtractive CNC stage found in UAM systems (right).

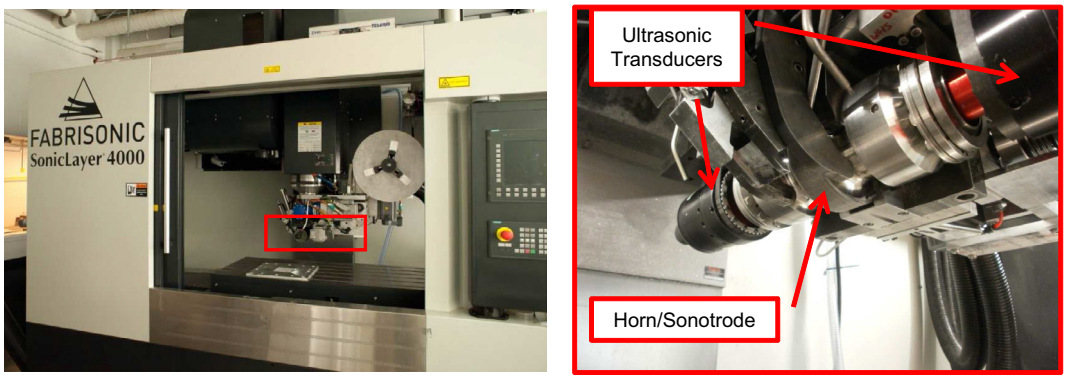

Fig. 2. Commercial 9 kW UAM system, Fabrisonic SonicLayer 4000. Reprinted with permission [22].

into the workpiece. This matter is discussed in Section 6. Conventional LTI models for ultrasonic systems lump the influence of shear force or load into the motional feedback of the entire system for control purposes [23], i.e., Van Dyke system representation [24]. Because the focus of the paper is to describe the system dynamics of the welder, i.e., sonotrode and transducers, it is required to explicitly express shear force as a system input. This alternative LTI model can be used for improved control strategies and energy transfer analysis for the UAM process.

The paper begins by describing how the process is currently controlled and how this control strategy relates to UAM welder performance. Then, the welder is described in terms of impedance relations in order to formulate the proposed system level LTI model. Experimental frequency response functions (FRFs) and operating performance of the welding assembly are then measured to verify that the system follows LTI behavior and to identify model parameters. Using the model combined with in-situ measurements, shear force and welder efficiency are estimated for standard Al 6061 welding procedures. The influence of process variables, i.e., amplitude, down force, and speed, on shear force and efficiency is then studied. Lastly, the high frequency velocity response of the welder and how the welder couples with the UAM part are investigated with the use of the LTI model.

2. UAM control background

UAM has been utilized for nearly a decade, yet the process uses legacy control strategies designed for ultrasonic metal welding of single metal joints. In UAM, many joints are made and the build geometry changes throughout component construction. Consequently, unwanted resonances can occur [25,26] and the amount of deformation at the weld interface effectively imparted by the welder decreases as the build becomes more compliant with added layers [27,28]. Due to less deformation occurring at the weld interface and because deformation is a leading mechanism for bonding, the bond quality degrades with additional layers. A control strategy unique to UAM is needed to avoid or minimize undesired structural dynamics and to maintain weld quality throughout component construction. Such a control strategy can be developed with a reliable system level model of the UAM process.

Fig. 3 demonstrates how the control dynamics of the UAM process change when welding vs. actuating the sonotrode without load, i.e., with no welding. In particular, the peak velocity of the scrubbing motion decreases 10% (Fig. 3(a)), the frequency of the welder increases 75 Hz (Fig. 3(b)), and the electric power draw of the piezoelectric transducers increases an order of magnitude, see Fig. 3(c). A customized ultrasonic generator for the UAM process is responsible for the control dynamics observed in Fig. 3. The generator uses two closed loop controllers which work simultaneously. The first controller uses a phase lock loop (PLL) algorithm to track system resonance during welding by minimizing the phase angle between the applied voltage and current [29,30]. System resonance can change when welding due to added mass, stiffness, and heat generation from the load [30–32]. This PLL algorithm is the reason for the upward frequency shift in Fig. 3(b), and this shift occurs due to the UAM build stiffening the system during welding.

The second controller works to maintain welder amplitude as the part is built, which under open loop conditions would result in a decrease in amplitude. Welder amplitude in UAM is maintained by controlling voltage to be constant. Voltage is controlled by varying the current to maintain a set-point value for a given amplitude setting [33]. Further detail on voltage control will be discussed in Section 4. Ultrasonic systems can be controlled using electric current in a similar manner [23,30].

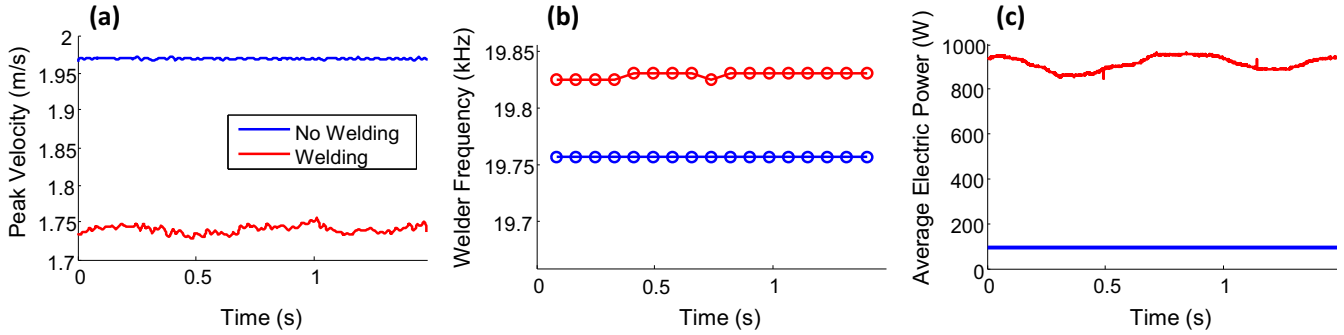

Fig. 3. UAM system dynamics and control when not welding, i.e., exciting welder in air without load, and welding Al 6061 foil: (a) peak sonotrode or welder velocity; (b) excitation frequency; (c) average electric power draw from one of the ultrasonic transducers. Data was collected using the welding process variables of 32.5 μm peak-peak prescribed welder vibration, a down force of 5000 N, and a rolling speed of 5 m/min (200 in./min). Data was sampled at 50 kHz and processed with a block size of 8192 points, welder vibration was measured with a non-contact laser vibrometer, welder frequency was obtained using a short time windowed FFT, and power draw was sampled directly from the ultrasonic generator.

In order to accurately track the resonance of the system for both the PLL algorithm and amplitude control, the mechanical motion of the welder needs to be measured. The most common way of measuring mechanical motion is with the use of motional feedback methods. Motional feedback works by adding a reactive element in series or in parallel with the transducer to balance out its electrical impedance or admittance [23,30–32]. For piezoelectric systems, this reactive element is an inductor. By balancing out the electrical impedance of the transducer, the motional impedance of the transducer can be indirectly measured with applied current and voltage to the transducer. There are many different circuits utilized to implement motional feedback control techniques [23,32]. The ultrasonic generator used on UAM systems utilizes such a motional feedback method for resonance tracking and amplitude control. Because amplitude is not measured directly in UAM, a decrease in vibration can occur if the reactive inductance element does not sufficiently isolate the motional impedance of the transducer or if significant compliance exists in the sonotrode, see Fig. 3(a). This decrease in welder velocity and its relation to motional feedback and sonotrode compliance will be discussed in more detail later. Lastly, because voltage is controlled to be constant by increasing electric current during welding, the average electric power draw increases substantially to maintain welder motion, see Fig. 3(c).

3. Time-invariant linear model of UAM process

To describe the system dynamics of the welder for all frequencies (ω), the following LTI system model with voltage-force as across variables and velocity-current as flow variables for the system can be written,

$$\begin{pmatrix} i(j\omega) \\ \dot{\delta}(j\omega) \end{pmatrix} = \begin{bmatrix} H_e(j\omega) & H_{me}(j\omega) \\ H_{em}(j\omega) & H_m(j\omega) \end{bmatrix} \begin{pmatrix} V(j\omega) \\ F_s(j\omega) \end{pmatrix}, \tag{1}$$

where H_e is the FRF between applied voltage (V) and electric current (i), H_{me} is the FRF between opposing shear force during welding (F_s) and current, H_{em} is the FRF between applied voltage and velocity of the sonotrode ($\dot{\delta}$), and H_m is the FRF between shear force and velocity. Due to the system being piezoelectric, the system follows the law of reciprocity [24,34]. As a result, H_{me} and H_{em} are nearly equal in magnitude and phase. Force as the across variable and velocity as the flow variable is proposed initially due to piezoelectric systems conventionally using this form [23,24,34], and because the system is feasible to characterize in this form. An equivalent LTI model of the system using velocity as the across variable and force as the flow variable will be presented at the end of this section because the motional feedback controller utilizes this relationship. The equivalent form is derived using the principle of duality [34]. Either formulation can be used to describe the system behavior because the system behaves in a steady manner during welding operations, as evidenced by the stable welding traces in Fig. 3. The system exhibits a small amount of variation when welding because the PLL algorithm moves the voltage excitation frequency. This small frequency shift in the PLL controller may originate from variations in the UAM build compliance and shear force character during welding. The influence of UAM build stiffness on frequency and FRF magnitude will be discussed in more detail in Section 8.

To understand the relationship between system physics and the FRF terms, equivalent circuit analysis can be used to derive closed form FRF expressions near resonance. To model the electromechanical coupling of the piezoelectric transducers, an ideal transformer can be utilized [24,35]. A schematic of the welding assembly along with its corresponding equivalent circuits are shown in Fig. 4. The equivalent circuit analysis is conducted assuming that the welding assembly is geometrically symmetric in shape and properties and that the two transducers operate out of phase, i.e., push-pull configuration. The system can be assumed to be geometrically symmetric because the sonotrode is precision machined, and the two transducers used to drive the sonotrode exhibit near identical response [36]. Because the system is geometrically symmetric and the transducers are operated out of phase, the transducers can be lumped together as a single transducer driving the sonotrode. The out of phase actuation of the welder is shown in Fig. 4(a) with opposing voltage directions. The sonotrode in Fig. 4(b) is modeled as a black box 2-port electrical network because (i) the transducers actuate the sonotrode at a different location than the shear force, and (ii) the design influence of the sonotrode on system performance is not considered in this paper. Because sonotrode design is not an aspect of this paper, Fig. 4(b) can be simplified by lumping the transducer and sonotrode dynamics together, see Fig. 4(c). These two devices can be lumped together because both the transducers and sonotrode are designed to resonate at the driving frequency of 20 kHz. The equivalent circuit in Fig. 4(c) is the Mason circuit representation for piezoelectric devices [24].

System FRFs can be derived from the equivalent circuit shown in Fig. 4(c) by shorting out one input at a time and relating system outputs [24],

$$H_e = \frac{i}{V} = j\omega C_t + \frac{\Phi_t^2}{j\omega M_t + D_t + \frac{K_t}{j\omega}}, \tag{2}$$

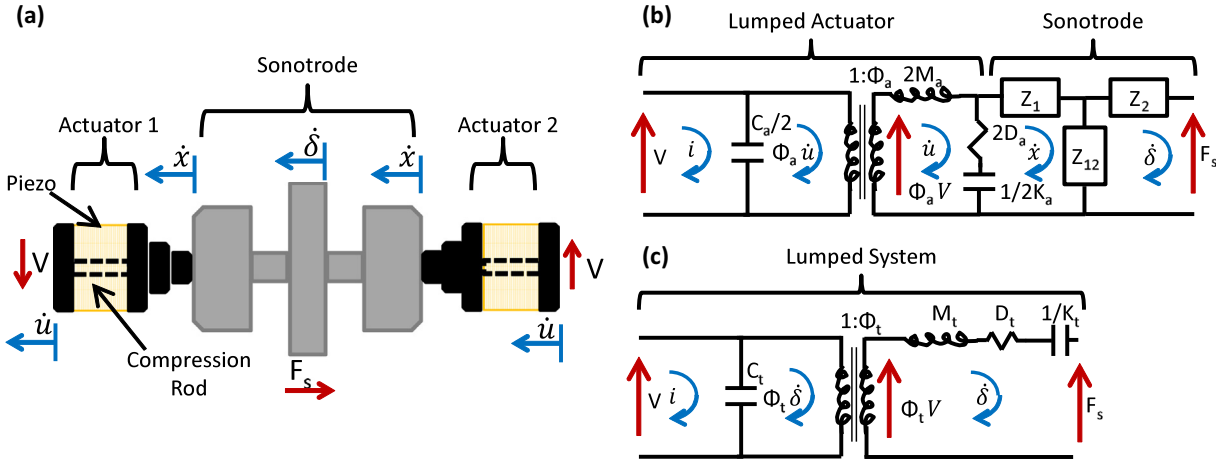

Fig. 4. UAM weld assembly analysis: (a) schematic of assembly with components, voltages, forces, and degrees of freedom detailed; (b) equivalent circuit of weld assembly with transducers and sonotrode modeled separately; (c) simplified equivalent circuit of weld assembly by lumping the transducers and sonotrode dynamics together.

$$H_{em} = \frac{\dot{\delta}}{V} = \frac{\Phi_t}{j\omega M_t + D_t + \frac{K_t}{j\omega}}, \tag{3}$$

$$H_m = \frac{\dot{\delta}}{F_s} = \frac{1}{j\omega M_t + D_t + \frac{K_t}{j\omega}}. \tag{4}$$

where C_t is the capacitance of the transducers, Φ_t is the electro-mechanical transformer coefficient or turns ratio of the system, M_t is the effective mass of the system, K_t is the effective stiffness of the system, and D_t is the effective damping of the system.

Using the principle of duality, the equivalent circuit in Fig. 4(c) can be redrawn using velocity as the across variable and shear force as the flow variable, see Fig. 5. This system form is called the mechanical mobility equivalent circuit of the system [34], and the welder utilizes it for control purposes. As mentioned earlier, motional feedback or purely electric signal feedback is utilized by the ultrasonic generator to maintain welder amplitude or velocity during welding. Motional feedback works by inserting an external inductor in series with the capacitive element of the transducer, see Fig. 5(a). If the impedance of the inductor is chosen to be equal to the capacitor impedance at resonance, the electrical impedance of the transducer is balanced out or removed from the circuit, see Fig. 5(b). By removing the capacitance of the transducer near resonance, the motional impedance of the transducer can be isolated for control purposes, hence the name motional feedback. Welder velocity is directly related to applied voltage too and can be used for amplitude control purposes.

An equivalent LTI model using current and shear force as inputs and velocity and voltage as outputs can then be written,

$$\begin{pmatrix} V(j\omega) \\ \dot{\delta}(j\omega) \end{pmatrix} = \begin{bmatrix} H_e^*(j\omega) & H_{me}^*(j\omega) \\ H_{em}^*(j\omega) & H_m^*(j\omega) \end{bmatrix} \begin{pmatrix} i(j\omega) \\ F_s(j\omega) \end{pmatrix}, \tag{5}$$

where H_e^* is the FRF between electric current and voltage (V), H_{me}^* is the FRF between shear force and voltage, H_{em}^* is the FRF between electric current and welder velocity, and H_m^* is the FRF between shear force and velocity. H_{me}^* and H_{em}^* are equal in magnitude and phase like the other LTI model of the welder. These FRFs can written in terms of lumped system parameters and assuming that the electrical impedance of the system is suppressed,

$$H_e^* = \frac{V}{i} = \frac{\Psi_t^2}{j\omega M_t + D_t + \frac{K_t}{j\omega}}, \tag{6}$$

$$H_{em}^* = \frac{\dot{\delta}}{i} = \frac{\Psi_t}{j\omega M_t + D_t + \frac{K_t}{j\omega}}, \tag{7}$$

$$H_m^* = \frac{\dot{\delta}}{F_s} = \frac{1}{j\omega M_t + D_t + \frac{K_t}{j\omega}}. \tag{8}$$

where Ψ_t is the electro-mechanical transformer coefficient of this equivalent form. The other lumped parameters are assumed to not be dependent on the particular equivalent circuit form because they influence the system resonance and system resonance is nearly identical between the two forms. The shear force and applied electrical current in (5) are out of phase at the 20 kHz driving frequency (ω_o) because shear force opposes welder vibration directly. This out of phase shear force can be expressed with a minus sign,

$$\dot{\delta}(j\omega_o) = H_{em}(j\omega_o) i(j\omega_o) - H_m(j\omega_o) F_s(j\omega_o). \tag{9}$$

Similarly for voltage,

$$V(j\omega_o) = H_e(j\omega_o) i(j\omega_o) - H_{me}(j\omega_o) F_s(j\omega_o). \tag{10}$$

Harmonic excitation is assumed in relations (9) and (10) to describe system dynamics at resonance. These relations will be used later in Section 5 of the paper to calculate welder shear force.

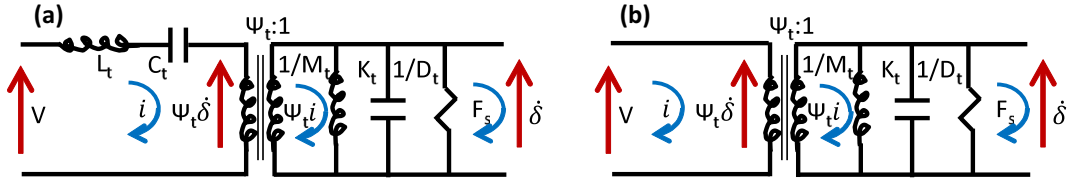

Fig. 5. Equivalent circuit for welder operation: (a) mobility form of system with added inductance to 'zero out' transducer capacitance; (b) simplified mobility form of system without electrical influences from transducer, i.e., motional feedback form.

Evidence supporting these relations will be presented in Section 7. Prior to using the model to estimate shear force and welder efficiency, it is of interest to show that the presented lumped system models are valid and can be used to describe UAM dynamics. Verification and identification of model parameters is carried out in the next section utilizing experimental FRF measurements and characterization techniques, respectively.

4. Welder characterization

4.1. Frequency response function measurements

To describe welder boundary conditions for FRF estimation, the welder was characterized inside the UAM machine, see Fig. 6. To apply a controlled voltage and measure electric current across the piezoelectric transducers, an AE Techron LVC 5050 was utilized. A Polytec PSV-400 Doppler laser vibrometer was used to measure sonotrode motion in a non-contact manner. The ability to measure welder vibration in a non-contact way is important because any added mass and geometry will adversely influence the tuned resonance behavior of the system. A high frequency modal hammer (PCB 086C30) was used to input a known force impulse into the sonotrode. A modal hammer was utilized because mass loading on the structure would be minimized compared to piezo reaction mass excitation. Lastly, a Data Physics QUATTRO Dynamic Signal Analyzer was used to estimate FRFs. The equipment used to characterize the welder is shown in Fig. 6 while a characterization schematic is shown in Fig. 7.

To measure H_e and H_{em}, one transducer was used to excite the system while the other was put into an open circuit condition. This characterization approach is valid because the system is symmetric, which makes the test conditions equivalent to driving the system with two transducers. Also, the open circuit condition is required to allow energy storage over the capacitor and to prohibit current flow out of the passive transducer. Because the resonance of the welder is lightly damped, swept sine excitation was utilized around the 20 kHz resonance. Frequency spacing during the sweep was 0.5 Hz and measurements were taken until a minimum ordinary coherence value of 0.99 was reached for the frequencies of concern. To measure H_m, both transducers were short circuited with low resistance stranded wire while the modal hammer was used to excite the sonotrode. The transducers were short circuited so that energy would not be stored within the capacitive element of the transducers. FRF estimation utilized 10 hammer impacts for averaging and an exponential processing window to minimize leakage error. Frequency resolution during H_m estimation was near 2.4 Hz, so measuring the peak FRF value was difficult.

Empirical FRFs are compared in Fig. 8(a) while the measurement of H_m for both transducers shorted, one transducer shorted, and no transducers shorted (open) is shown in Fig. 8(b). The FRF with the largest magnitude is H_e, followed by H_{em}, and then H_m in Fig. 8(a). It is shown in Fig. 8(b) that the magnitude of H_m is similar for each electrical boundary condition, but the resonant frequency changes. This resonant frequency dependence on the electrical boundary condition is typical for piezoelectric devices because the piezoelectric crystal stiffness is different for an open and short circuit condition [37]. Consequently, the resonant frequency of H_m does not coincide with H_{em} during testing. When the capacitive element is shorted, it is analogous to making the system less stiff, which causes a downward frequency shift. On the other hand, if the capacitive element is put into an open circuit state, the capacitance stiffens the system and causes an upward frequency shift. During welder operation, the electrical boundary conditions for the transducer are not shorted nor left open. Instead, it is a mixture of the two boundary conditions, which coincides with the H_{em} resonance. Consequently, for comparison purposes in Fig. 8(a), H_m is manually moved to coincide with H_{em}.

The Mason circuit model of the welder is compared to experimental FRFs in Fig. 9. The Mason circuit model was found using the measured FRF forms discussed earlier and with procedures given for an ideal Mason circuit [24]. The H_e FRF was used to estimate the system capacitance, mass, stiffness, and damping. The electro-mechanical transformer coefficient is found via the ratio of the mobility loop diameters of H_{em} and H_e. As shown in the Figure, the model and experiment demonstrate good correlation in magnitude with some error in phase. Phase error is believed to originate in the linear amplifier used to make the voltage and current measurements because 20 kHz is near the operating limit of the device. Consequently, phase error on the order of 15 degrees is possible [38]. Lumped model parameters for the Mason circuit are listed in Table 1.

4.2. Welder operation measurements

Because the measured system FRFs agree well with a lumped parameter model, it can be inferred that the mechanical mobility representation of the welder shown in Fig. 5 is also valid. To characterize this mechanical mobility representation of the welder, velocity, voltage, and average electric power measurements were made on the welder while it was operating without load. These

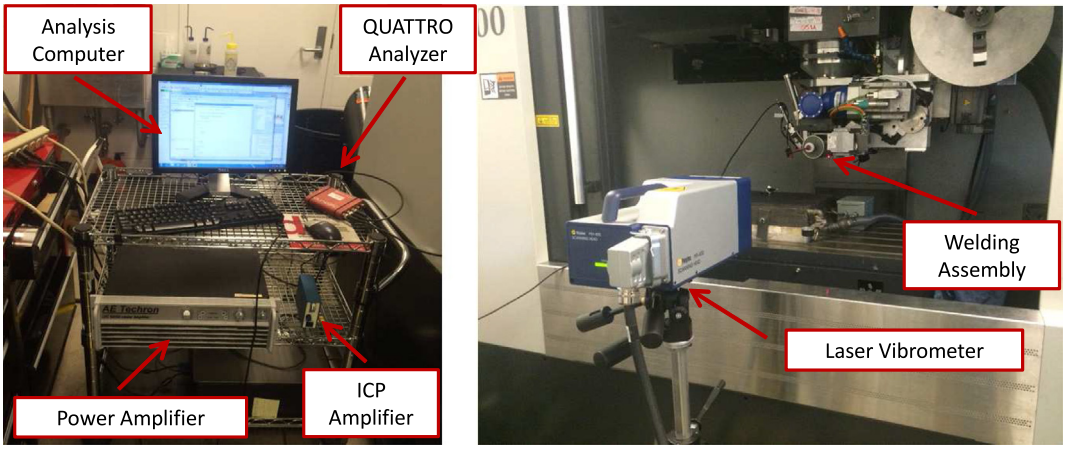

Fig. 6. Approach and equipment used to measure experimental FRF measurements of weld assembly. Characterization was done inside the UAM machine to emulate operating boundary conditions.

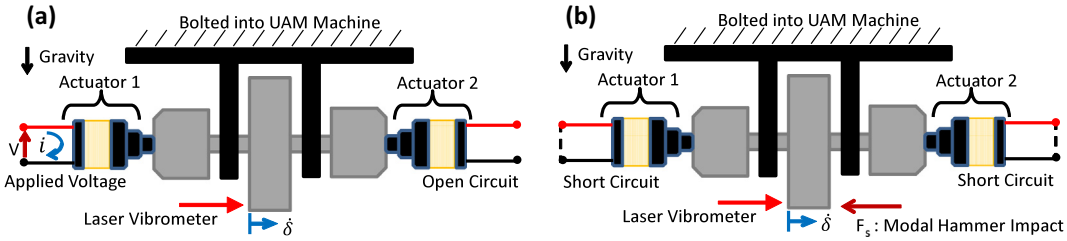

Fig. 7. Conditions for assembly FRF measurements: (a) H_e and H_{em} measurements by driving one transducer and leaving the other open; (b) H_m measurement by shorting both transducers with a low resistance stranded wire.

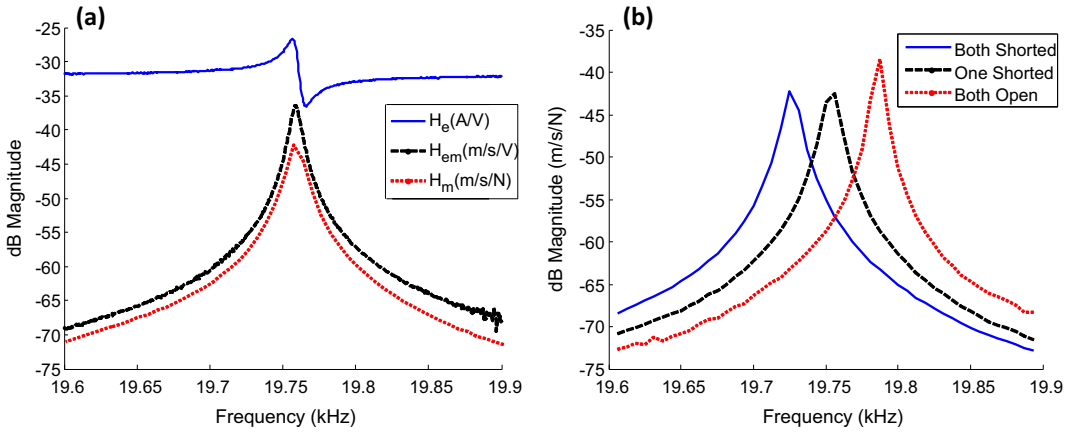

Fig. 8. Experimental FRF measurements of weld assembly near 20 kHz: (a) comparison of H_e, H_{em}, and H_m FRFs; (b) H_m resonance dependence on shorted and open circuit conditions. The system resonance is different for short and open circuit conditions because the piezoelectric crystal stiffness is different between the two electric boundary conditions.

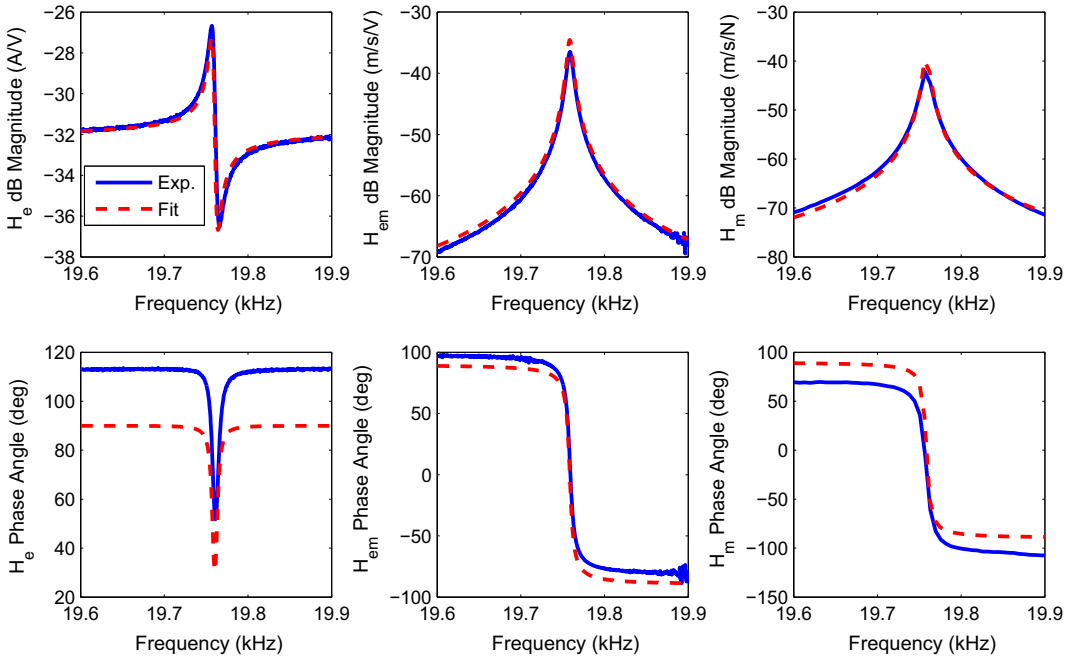

Fig. 9. Welder FRF comparison between measurement and system level model.

three variables were evaluated at different amplitude settings of the ultrasonic generator. To measure welder velocity, the noncontact laser vibrometer was utilized. A Tektronix P6015A voltage probe was used with an Agilent 54622A oscilloscope to measure RMS voltage and P-P voltage of the welder. Power was measured by using the analog output channel on the ultrasonic generator.

To obtain accurate estimates for system voltage and power, the welder was driven with one transducer while the other was left in the open circuit condition. By driving the system with one

Table 1
Lumped parameter values for Mason circuit model of welder.

Model variable	Value
C_t (nF)	203.21
M_t (kg)	1.98
K_t (GN/m)	30.49
D_t (Ns/m)	82.05
Φ_t (N/V)	1.54

transducer, the ultrasonic generator doubles the applied current to achieve the same voltage and welder velocity outputs [36]. Because current doubles and the voltage is constant, the power also doubles. Peak welder velocity and average electric power draw for the amplitude levels of 40%, 50%, 60%, 70%, and 80% are shown in Fig. 10(a) while peak voltage is shown in Fig. 10(b). It was found that the measured applied voltage was very similar to a sine wave, so the voltage in Fig. 14(b) was scaled by the RMS coefficient $\left(\frac{1}{\sqrt{2}}\right)$ for a sine wave. As shown in Fig. 10(a), peak welder velocity changes linearly with amplitude setting while average weld power changes in a quadratic manner. Peak welder velocity is expected to change in a linear manner with applied voltage when no shear force is present, see (5). Likewise, voltage also changes linearly with the amplitude setting when there is no shear force present. Power, on the other hand is expected to change quadratically because it is a function of current squared when shear force is not present.

As a result of the voltage and velocity changing linearly together in Fig. 10, the coupling constant for the mechanical mobility representation of the welder (Ψ_t) can be found by fitting a line between the two variables. As shown in (6)–(8), Ψ_t is scaled by the mechanical admittance (H_m^*) to estimate H_{em}^*. As a result, applied peak current can be estimated by using Ψ_t, H_m^*, and measured peak welder velocity. Estimated peak current can then be used with measured RMS voltage to calculate average electric power, $P_{e,avg}$. Average electric power is defined as the multiplication of RMS voltage, RMS current, and the cosine of the phase angle (θ) between voltage and current,

$$P_{e,avg} = V_{RMS} i_{RMS} \cos\theta. \tag{11}$$

The H_e^* transfer function theoretically does not have a resonance and an anti-resonance in UAM because motional feedback is used. Instead, the function will behave more like a single degree of freedom model and have a phase angle of zero at resonance, see (6). Thus, the phase angle between applied current and voltage can be assumed to be zero in (11). Using this phase angle simplification, the average electric power can be estimated and compared to the measurement, see Fig. 11. The estimated power is higher than the measurement. To remedy this mismatch, the peak magnitude value of H_m^* was adjusted by increasing it 12%. As a result of the peak value of H_m^* being difficult to accurately measure during characterization, increasing its value is likely more accurate as well. With this adjustment to H_m^*, the power estimate shows closer agreement with the measured value. The calculated constants utilized for this power calibration are listed in Table 2.

In addition to estimating power, the excitation frequency of the welder was compared to FRF measurements. This excitation frequency was found using the measured welder velocity signal and FFT algorithm within Matlab. The excitation frequency as a function of amplitude setting is shown in Table 3. It was found that the excitation frequency of the system was identical or very near the resonance of the system during FRF characterization. The small variation in excitation frequency is believed to originate in the frequency resolution of the processing block size to calculate the frequency.

5. Shear force estimates and welder efficiency

The welder calibration results in Fig. 11 were calculated assuming that welder current, voltage, and velocity signals were single frequency (ω_o), i.e., sine waveforms. It was also assumed that the phase angle between the applied current and voltage is zero due to the PLL algorithm. Using these assumptions, (11) can be simplified to the following,

$$P_{e,avg} = \frac{1}{2} V i. \tag{12}$$

Eq. (12) is a reasonable simplification for average electric power draw considering that the 1st harmonic of the weld velocity is an order of magnitude greater than all other higher order harmonics (see Figs. 17 and 21 in Section 7). Because applied voltage to the piezoelectric transducers is controlled to be constant for a given amplitude set-point value, the ratio of average electric power between two welding layers or states can be equated to the ratio of weld currents,

$$\frac{P_2}{P_1} = \frac{i_2}{i_1}, \tag{13}$$

where P_2 and P_1 are the average electric power for welding states 2 and 1, respectively. Likewise, i_2 and i_1 are the applied peak electric current values for welding states 2 and 1. Using estimated current from the model and measured average electric power for not welding (state 1), applied current during welding can be estimated if average electric power draw is measured (state 2). With this

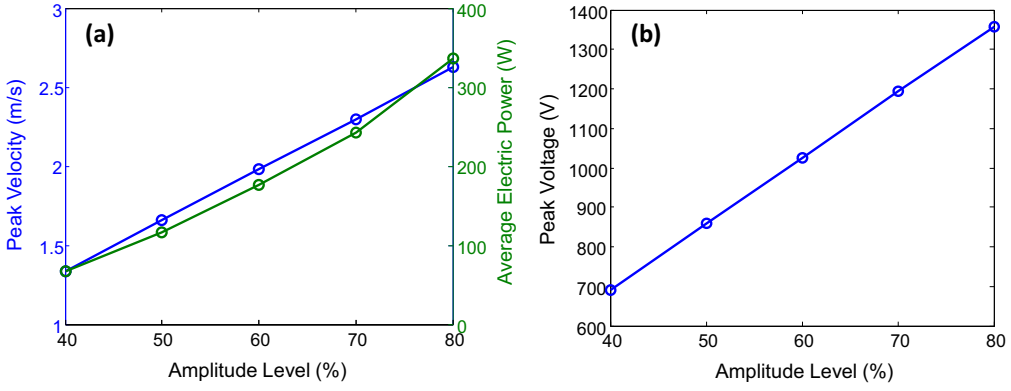

Fig. 10. Operation of welder operating under no load, i.e., not welding: (a) comparison of peak welder velocity and average electric power draw as a function of amplitude setting; (b) applied voltage as a function of amplitude setting.

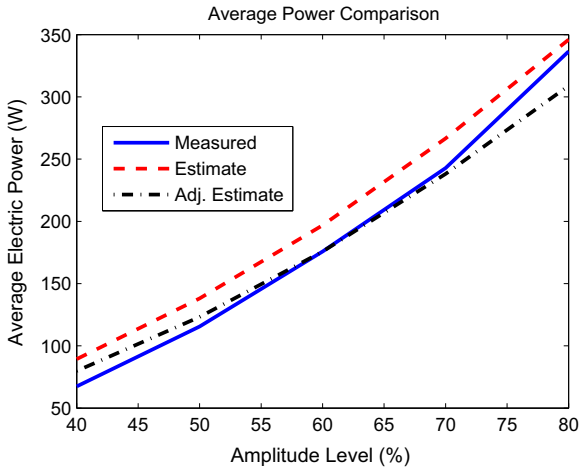

Fig. 11. Calibration of mechanical mobility model to average electric power.

Table 2
Coefficients used to validate mechanical mobility representation.

Model variable	Value
Ψ_t (V∗s/m)	515.3
Peak H_m^* (m/s/N)	0.010
Adjusted peak H_m^* (m/s/N)	0.0112

Table 3
Frequency of welder velocity as a function of amplitude level. Frequency found via windowed FFT with frequency resolution near 3 Hz. The median frequency of 19.757 kHz agrees well with FRF measurements. A Hamming processing window was utilized to minimize leakage when estimating frequency.

Amplitude setting (%)	Frequency (kHz)
40	19.760
50	19.757
60	19.757
70	19.754
80	19.754

estimate for applied current at the excitation frequency, welder shear force can then be estimated using the LTI model, assuming operation at resonance (9) and (10), and using measured peak welder velocity,

$$F_s = \frac{H_{em}^* i - \dot{\delta}}{H_m^*}. \tag{14}$$

To illustrate the use of (14), the states of not welding and welding can be compared, see Fig. 12. Along with estimated shear force between the two states, the measured average electric power, measured peak welder velocity, and calculated excitation frequency are also shown in the figure. In-situ measurements were sampled at 50 kHz (25 kHz Nyquist) with a National Instruments DAQ module. Consequently, content in Fig. 12 is from the excitation signal (near 20 kHz) and contains no higher order harmonic content. The average electric weld power increases an order of magnitude, the welder excitation frequency increases 75 Hz, the peak welder velocity decreases 10%, and shear force is near 1750 N during welding. Shear force during ultrasonic spot welding has been measured previously [39], and found to be near 1800 N for the same aluminum alloy with a similar sonotrode contact area.

The shear force of the welder exhibits similar behavior to the average electric power in Fig. 12 since (13) is used to estimate applied current to the welder. The reported average electric power in the figure was measured from a single piezoelectric transducer and doubled in value because power draw is near symmetric between the two transducers on the sonotrode.

With the use of estimated peak shear force, measured peak welder velocity, and measured average electric power draw, welder efficiency (e) can then be calculated,

$$e = \frac{P_{m,avg}}{P_{e,avg}} = \frac{\frac{1}{2}\dot{\delta}F_s}{P_{e,avg}}. \tag{15}$$

Welder efficiency is calculated using the ratio of average mechanical power ($P_{m,avg}$) and average electric power ($P_{e,avg}$). This efficiency calculation was carried out with the assumption that the majority of the applied electrical energy is concentrated near the excitation frequency as well. Efficiency comparisons between the states of not welding and welding are shown in Table 4. The efficiency is not exactly zero when not welding because there is a small residual shear force from the calculation (14). Nonetheless, the estimated welding efficiency is near estimates for ultrasonic metal welding systems [6] and below that of UAM piezoelectric transducers [40], which is greater than 90%. This estimate is sensible considering efficiency cannot be greater than the ultrasonic transducers themselves. Losses in the system which decrease efficiency are bushings, bolted joints, material damping within the waveguide, and friction in the spring diaphragm ball bearing. Additionally, some error in the efficiency and shear force measurement may be attributed to higher order harmonics not being considered in the calculation. The effect of higher order harmonics is discussed in Section 7.

6. Influence of UAM processing conditions on shear force and efficiency

In addition to comparing the shear force and efficiency estimates between the states of not welding and welding, the influence of UAM processing conditions on these estimates can be evaluated. The influence of welder amplitude or velocity on system dynamics is shown in Fig. 13 while the efficiency for the amplitude levels of 40%, 50%, and 60% are listed in Table 5. These measurements were made while all other processing variables were held constant and at the same number of UAM weld layers. This same procedure was done when evaluating normal force and speed.

As shown in Fig. 13, the average electric power draw increases with amplitude level, the peak welder velocity increases monotonically with amplitude setting, the excitation frequency decreases with higher amplitude levels, and shear force increases with higher amplitude levels. Power draw and shear force increases with amplitude level because enhanced motion increases both elastic and plastic deformation of the system. This increase in deformation leads to a corresponding increase in effort from the welder. The efficiency decreases with larger welder amplitude levels because plastic deformation and some slip is present during UAM. The relationship is made more clear by evaluating the closed form relation of efficiency in terms of welder motion and shear force,

$$e = 1 - \frac{\dot{\delta}}{\dot{\delta} + H_m^* F_s}. \tag{16}$$

If the shear force and welder motion are not linearly related, the efficiency can show some variation. Since metal plasticity and slip are present in UAM, it is suspected that their non-linearity is the reason for the efficiency variation in Table 5.

The next UAM processing variable to be evaluated is the normal or down force. Results for the normal force levels of 4000, 5000, and 6000 N are shown in Fig. 14 and Table 6. These different normal force levels do not strongly influence UAM system dynamics from one level to the next because it has been shown that frictional slip does not strongly influence UAM at these force levels [11,22].

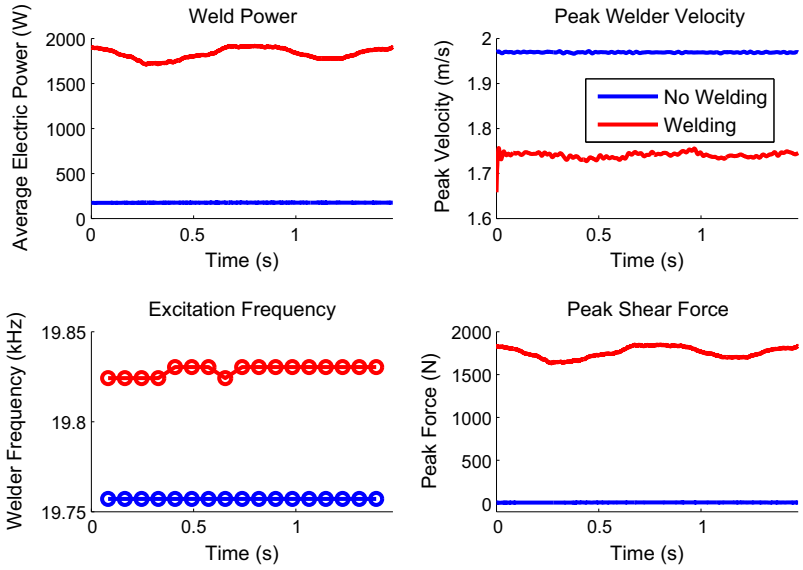

Fig. 12. Estimate of welder shear force from in-situ velocity and power measurements. Welder excitation frequency is also compared to illustrate system stiffening when welding.

Table 4
Welder efficiency comparison between the states of not welding and welding. A small efficiency is calculated for the state of not welding due to a small residual shear force being present from the calculation of shear force (14).

	No welding	Welding
Mean	4.31	83.66
Std. dev.	0.50	0.44

Negligible magnitude difference is observed between the average electric power draw and peak shear force for the different force levels. Peak welder velocity decreases near 1.5% between each force level and excitation frequency decreases in an exponential manner with normal force level. An explanation of this observed trend can be described by evaluating the inductor impedance (L_t) used in the motional impedance control strategy [23],

$$L_t = \frac{1}{\omega^2 C_t}. \tag{17}$$

If the inductance used to cancel out the electrical impedance of the transducer is fixed during welding, velocity will not be held constant because excitation frequency changes. Down force may influence the coupling of the welder to the build, which then ultimately influences the excitation frequency of the welder. This welder amplitude influence would then make the system less efficient since energy is being stored in the capacitor. This reasoning is supported by the decrease in efficiency in Table 6.

The last UAM processing variable to evaluate is linear weld speed or how quickly the sonotrode rolls along the surface of the UAM build during construction. Results for the speed levels of 3.75 (150), 5.00 (200), and 6.25 m/min (250 in./min) are shown in Fig. 15 and Table 7. These weld speed levels have little to no influence on welder performance or efficiency. This observation

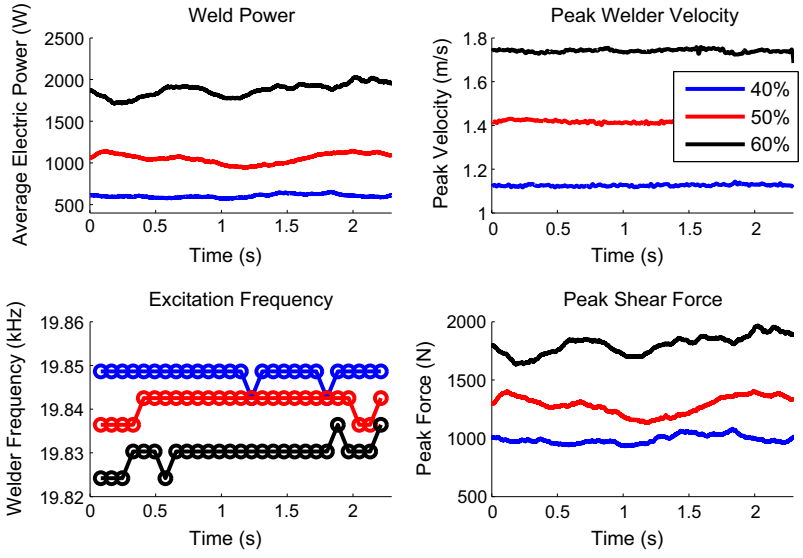

Fig. 13. Comparison of system dynamics as a function of amplitude level. Other UAM processing conditions were held constant in this study. In particular, normal load was 5000 N, linear weld speed was 5 m/min (200 in./min), and welds were made at room temperature.

Table 5
Welder efficiency comparison between different amplitude settings.

	40%	50%	60%
Mean	92.4	86.2	83.7
Std. dev.	0.53	0.43	0.47

corroborates other 9 kW UAM experimentation [22] and energy transfer models [28] because slower weld speeds (V_t) were found to linearly improve bond quality. In other words, the imparted energy to the weld interface (E_{welder}), and ultimately bond quality, is linear with speed because imparted mechanical power (P_{mech}) is not a function of welder speed within the investigated speed range,

$$E_{welder} = \frac{x}{V_t} P_{mech}, \tag{18}$$

where x is the linear travel distance of the welder.

7. Welder velocity response during UAM

The following sections discuss the influence of shear force and build compliance on welder velocity response during UAM. The first section discusses why welder shear force influences harmonic content in the velocity spectrum of the welder. The second section examines the effect of UAM build compliance on the nominal excitation frequency and the harmonic content magnitude.

7.1. Effect of shear force

As discussed in Section 2, the ultrasonic generator utilizes a phase lock loop algorithm combined with motional feedback to maintain a prescribed welder vibration magnitude and to track system resonance shifts during UAM. The relationship between build stiffness and excitation frequency shifts were discussed in detail while the control framework for constant amplitude control at the nominal excitation frequency was explained. It was not explained that additional frequency content exists in the velocity response during welding, see Fig. 16. Specifically, the lateral scrubbing velocity response of the welder increases at all frequencies and exhibits content at harmonic locations of the excitation frequency. This harmonic content has been observed prior in UAM [29] and in ultrasonic spot welding [41], yet its origin has not been fully explained.

The frequency response of the welder velocity is different during welding vs. not welding because the shear force input function contains energy at all other frequencies in addition to the nominal excitation signal. The exact excitation frequency of the welder depends on the effective resonance of the sonotrode and transducers, as explained earlier. To explain why additional frequency content exists in the welder velocity signal, the proposed LTI model expression (5) can be used to describe the velocity response for all frequencies,

$$\dot{\delta}(j\omega) = H^*_{em} i + H^*_m F_s. \tag{19}$$

Eq. (19) explains that welder velocity can be represented as a linear combination of the applied electric current and resultant shear force for all frequencies. It was established in Section 5 that the electric current used to actuate the welder could be approximated as a sine wave because the measured welder output voltage was found to be nearly sinusoidal. This single tone excitation is corroborated when analyzing the velocity response of the welder when operating under no load because its response is also sinusoidal, Fig. 4(b). Because the excitation signal is concentrated near resonance (ω_o), content at other frequencies must come from the shear force input function. Further, the observed content in the velocity spectrum is originally passed through the system transfer path or frequency response function (FRF) for a given system input. These FRFs act as filters on the system, and they influence frequency content in the velocity spectrum. To understand FRF influence on velocity and system response at high frequencies, these functions can be measured.

Obtaining FRF measurements at frequencies above 20 kHz is difficult. For measuring H^*_m, state-of-the-art high frequency modal hammers do not exhibit the necessary frequency response to reliably characterize the system upward of 20 kHz. For measuring H^*_{em}, response above resonance is low and narrow band excitation techniques are required. Despite these measurement difficulties, the general character of the FRFs can be investigated, see Fig. 17. The FRFs in the figure were obtained using the procedures outlined in Section 4 and using the built-in high frequency data acquisition system of the laser vibrometer. It should be noted that H_{em} in

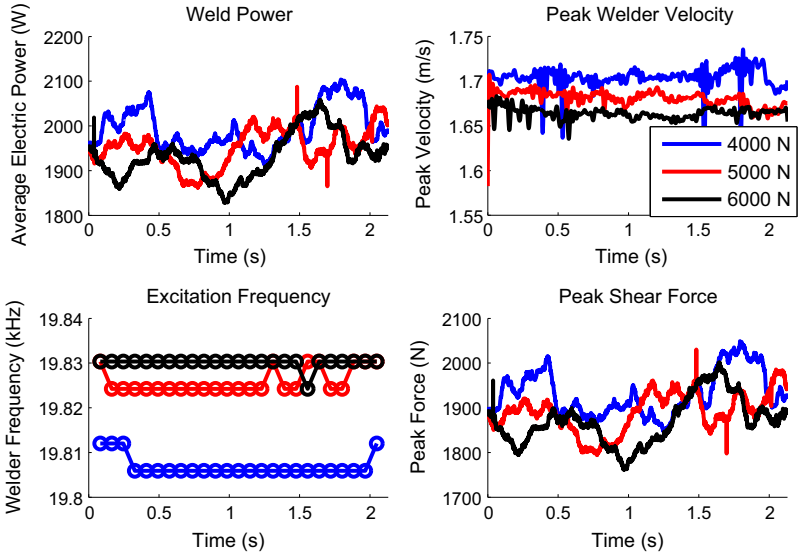

Fig. 14. Comparison of system dynamics as a function of normal force. Other UAM processing conditions were held constant in this study. In particular, prescribed welder amplitude was 60% (32.5 μm), linear weld speed was 5 m/min (200 in./min), and welds were made at room temperature.

Table 6
Welder efficiency comparison as a function of normal force.

	4000 N	5000 N	6000 N
Mean	82.48	81.34	80.56
Std. dev.	0.60	0.36	0.36

Fig. 17 is for the velocity-voltage FRF (H_{em}) and not the velocity-electric current FRF (H^*_{em}). However, the two FRFs have similar behavior and can be used for comparison purposes.

The harmonic locations of the nominal resonance of 19.757 kHz are marked in Fig. 17 with asterisks. Aside from the excitation harmonic (1st), the harmonics of the excitation signal do not coincide with any other system resonances. Consequently, significant amplification of harmonic content is not suspected during welding, and the content in Fig. 4(b) must be transmitted at low response regions of the H^*_m FRF. Because harmonic content is transmitted at low response regions, the origin of the content must come from the shear force excitation function.

7.2. Effect of build compliance

Prior work by the authors [28] has shown that UAM build compliance influences the performance of the process and ultimately part quality. To maintain performance and part quality in UAM, the concept of power compensation was presented. Compensated power is when the welder displacement is increased manually to maintain a constant electric power input into the UAM build due to build compliance influencing the welder effort to reach a prescribed amplitude limit. Uncompensated means that the welder amplitude is not adjusted during build construction, i.e., default constant amplitude control of the welder is utilized. The concept of power compensation is shown schematically with corresponding measurements in Fig. 18. Hehr et al. [28] did not investigate welder velocity content during this study. Consequently, the impact of build compliance and power compensation on the harmonic content in the velocity spectrum was studied herein using in-situ welder velocity measurements as a function of build height.

Fig. 18(a) illustrates why UAM build compliance impacts the process while measured average electric weld power is shown in Fig. 18(b). Fig. 18(c) illustrates the hypothesized bilinear shear force input function and plasticity behavior of the weld foil during the UAM process. The shear force or reaction force from the UAM build changes linearly with build stiffness (k) until the yield strength (F_y) of the foil is reached. Then, the weld foil plastically deforms with a constant tangent stiffness (k_T) to the prescribed welder amplitude value or displacement limit (δ_L). Because the stiffness of the build decreases with build height, the amount of plastic deformation also decreases due to it taking more elastic deformation (δ_E) to initiate yielding. More details on this idea can be found in previous work by the authors [28].

Power compensation is carried out manually by increasing the prescribed amplitude limit each layer due to state-of-the-art UAM equipment not exhibiting a constant weld power feature. The approach used to keep power constant is listed in Table 8 and is similar to the approach used in previous work [28]. To measure average electric power draw as a function of weld height, the analog output signal for weld power on the ultrasonic generator was synchronized with welder velocity. Average electric power as a function of build height is shown in Fig. 19(a) with first standard deviation error bars about a mean value for a given layer. Because welder velocity is measured, welder frequency as a function of build height can be estimated using Fourier analysis, see Fig. 19(b). Welder frequency was found by using the FFT function in Matlab, a Hamming processing window to minimize leakage error, a 50% overlap, and a block size of 81920 (6.5 Hz resolution). Because the ultrasonic generator changes the frequency slightly during welding, first standard deviation error bars are used to show frequency variation about a mean value for each weld layer.

It is shown in Fig. 19(b) that welder excitation frequency shifts downward with more layers and with more displacement (compensated trace). The downward frequency shift for amplitude control (uncompensated trace) corresponds to the UAM build becoming less stiff with more layers. Because the build becomes less stiff with more layers, the amount of plastic deformation hardening decreases and leads to a decrease in the effective build stiffness. On the other hand, the increased displacement for power compensation increases this downward frequency shift. This increased frequency shift occurs because the effective build stiffness decreases with more plastic deformation. Additional evidence of this downward shift due to a larger amount of plastic deformation is shown in Fig. 13 when the influence of welder amplitude on

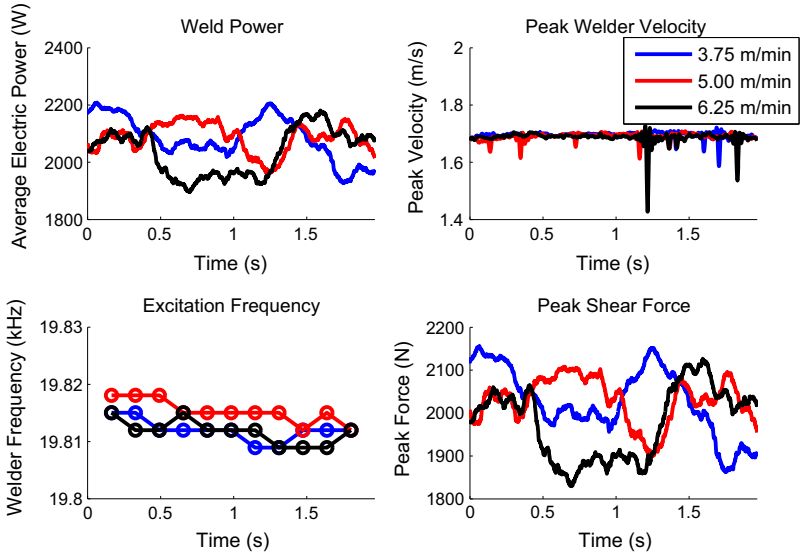

Fig. 15. Comparison of system dynamics as a function of weld speed. Other UAM processing conditions were held constant in this study. In particular, prescribed welder amplitude was 60% (32.5 μm), normal force was 5000 N, and welds were made at room temperature.

Table 7
Welder efficiency comparison as a function of weld speed.

	3.5 m/min	5 m/min	6.5 m/min
Mean	82.40	82.14	81.81
Std. dev.	0.61	0.62	1.10

shear force magnitude was evaluated. These two frequency shift mechanisms are schematically detailed in Fig. 20.

In addition to analyzing the frequency shift of the excitation signal as a function of build height, harmonic frequency content was examined. The dependence of this harmonic content on prescribed displacement and build stiffness can give insight into shear force and plasticity behavior of the weld foil during build construction. Averaged frequency content for the first three harmonics are shown in Fig. 21 for the compensated and uncompensated power conditions. This data was obtained by utilizing a Hamming processing window to simultaneously minimize leakage error and obtain accurate amplitude estimates. A 50% processing block overlap was also used. The processing block size was 81,920 points (6.5 Hz resolution), and this block size provided an adequate number of averages to statistically separate the trends shown in the figure. Because the processing frequency resolution was not extremely fine and the frequency is non-stable during UAM, points at and around the harmonic locations were used to estimate content by averaging them together for a given processing block. Three points were taken above and below the harmonic peak for averaging. Thus, seven total points were averaged together to produce the data shown in Fig. 21 with the first standard deviation as error bars.

The nominal excitation frequency content (20 kHz) is very steady for the uncompensated trace in Fig. 21(a). This steadiness is expected due to the ultrasonic generator attempting to keep amplitude constant during build construction. The cyclic variation shown in the uncompensated trace originates from periodically moving the measurement point of the laser vibrometer every 5 layers to remain on the sonotrode combined with the deformation behavior of the sonotrode. Sonotrode deformation behavior will be discussed in more detail in Section 8. The increasing content in the compensated trace is expected due to the velocity or amplitude increasing during build construction. It is shown in Fig. 21(b) that the 2nd harmonic content (40 kHz) is constant as a function of build height for both the compensated and uncompensated traces. This constant content implies that the hardening behavior (sawtooth component) of the weld metal does not change significantly with build height. On the other hand, the magnitude of the 3rd harmonic (60 kHz) demonstrates a large amount of change with the number of weld layers, see Fig. 21(c). Like the excitation frequency shift in Fig. 19(b), the compensated and uncompensated traces show decay as a function of build height. The decay in the content is expected because it is the first square wave harmonic and is the most sensitive to square wave changes, i.e., non-constant build compliance. Consequently, the increasing build compliance of the UAM stack with height influences the shear force profile.

The decreasing magnitude of the 3rd harmonic or square wave harmonic combined with the prevalent high order odd harmonics in Fig. 16(b) and transfer path character of H_m^* (see Fig. 17) can be used to hypothesize the shear waveform behavior during welding, see Fig. 22. The proposed forcing function exhibits predominant square waveform behavior because the dominant high frequency harmonics in Fig. 16(b) coincide with odd harmonic frequency content (60 and 100 kHz peaks). It is suspected that some plastic deformation hardening does exist in UAM as originally depicted in Fig. 18(c) because the sawtooth wave or even harmonic locations in Fig. 16(b) have content, but this content is much less than the square wave content and shows no change with build height. The square wave content changes with build height because the elastic stiffness of the build decreases and influences the shear force input function. In particular, the forcing function becomes less square wave like due to the build becoming more compliant with each added layer, which in turn reduces the magnitude of the 3rd harmonic with each layer. Fig. 22 illustrates the proposed force waveform behavior with k_1 representing a stiff UAM build while k_2 represents a less stiff build. The k_1 profile is more square like than k_2.

8. Discussion

A linear time invariant model of the UAM process has been proposed to describe process dynamics, see Fig. 3. In particular, the model explicitly specifies welder shear force as a system input to describe system dynamics and power conversion within the welder. This model was explored through equivalent circuit analysis, empirical FRF estimation, and characterization measurements

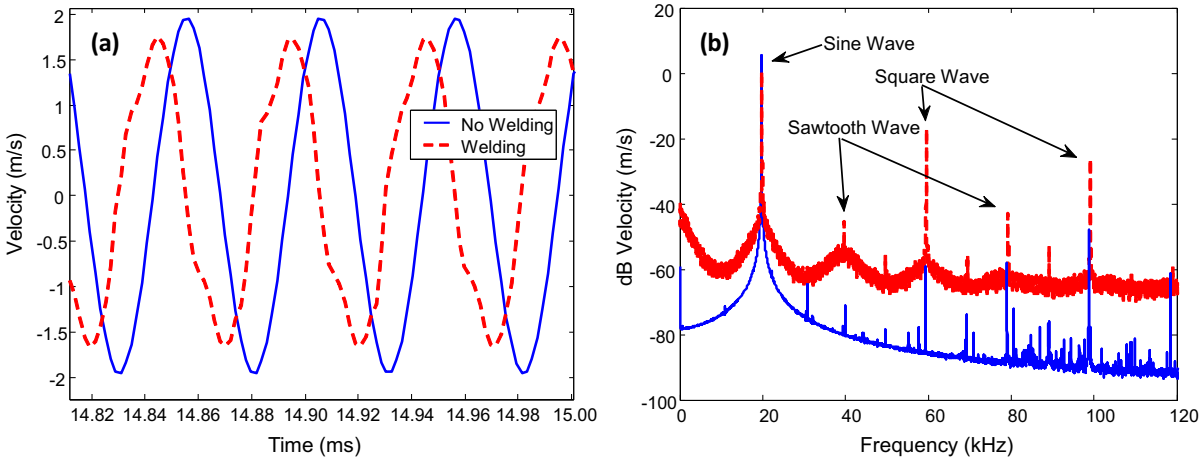

Fig. 16. Sonotrode or welder velocity character during UAM compared to actuating the welder without load, i.e., not welding: (a) time history comparison of signals; (b) frequency domain comparison of signals. Signals were sampled at 512 kHz with an amplitude level of 60% (32.5 μm setpoint). The phase delay in (a) is of no significance. The small decrease in welder amplitude during welding will be discussed in Section 8. Frequency data was obtained by averaging the velocity signal magnitude with a block size of 81,920 points and without windowing. Windowing was not used to illustrate increased frequency content more clearly. Due to windowing not being used, some leakage may be present in the figure.

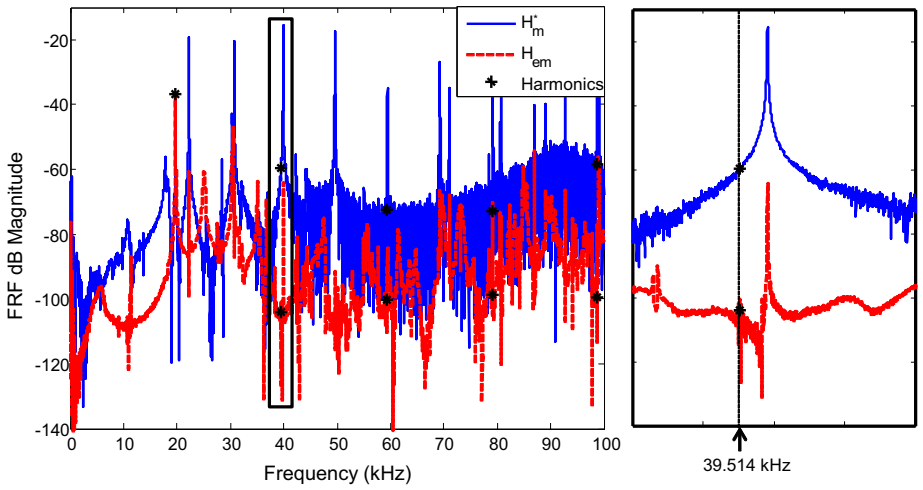

Fig. 17. H_{em} and H_m^* FRF estimates of the welder from 0 to 100 kHz. The nominal resonance of the welder is 19.757 kHz, and its harmonics are marked with asterisks on the FRFs. The 2nd harmonic (39.514 kHz) is given as an example. The locations of the harmonic frequencies were investigated to see if they coincided with any system resonances. No harmonics showed correlation with system resonances, so amplification is not significant during welding. FRFs were estimated using the built-in data acquisition of the Polytec laser vibrometer system.

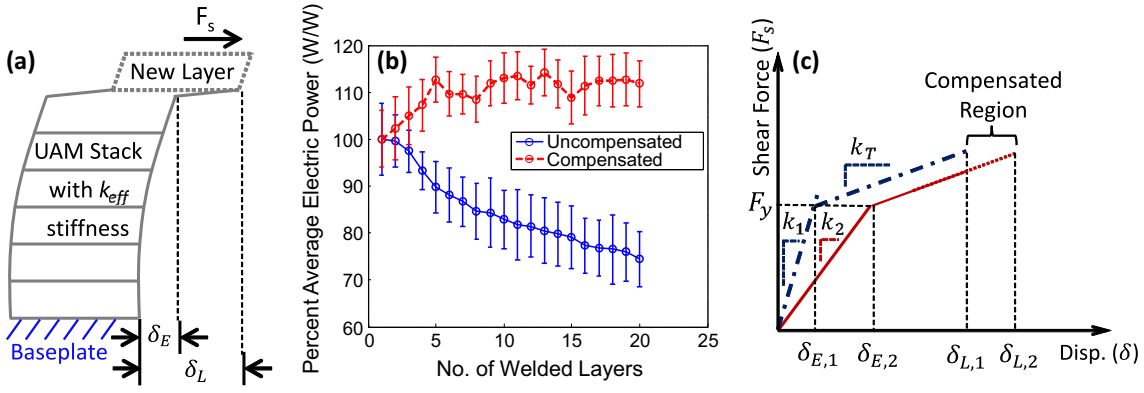

Fig. 18. UAM build dynamics: (a) schematic of UAM build during welding showing areas of elastic and plastic deformation; (b) comparison of measured average electric power draw percent for build with (compensated) and without (uncompensated) power control, reprinted with permission [28]; (c) proposed bilinear shear force profile during welding.

Table 8
Power compensation approach by increasing prescribed peak-to-peak displacement (δ_L) of the welder. Amplitude percentage was input into the machine controller to achieve the given displacement.

Layer	1–2	3–4	5–6	7–8	9–10	11–15	16–20
Amp. (%)	60	61	62	63	64	65	66
P-P δ_L (μm)	32.5	33	33.6	34.1	34.7	35.2	35.8

to understand system behavior and to identify system parameters. With this LTI model, shear force magnitude and welder efficiency were estimated for standard welding procedures for Al 6061 foil. The impact of welding variables on shear force and efficiency was also investigated. This model also provides insight into describing the high frequency harmonic content, the resonant frequency shift during welding, the decrease in welder amplitude under load, and can be used to describe the influence of UAM build dynamics on welder behavior.

8.1. Welder frequency and amplitude

UAM system dynamics change during welding because the dynamics of the weld assembly couple with the dynamics of the UAM build. The UAM build generates an opposing shear force which acts on the sonotrode, and the build stiffens the system due to the resonant frequency shifting upward. System stiffening can only occur if the sonotrode and the weld foil are not slipping on preceding layers when welding. Instead of slipping, it is believed that a psuedo-steady stick condition occurs because a stable upward frequency shift is observed when welding, Fig. 3 (c). If the sonotrode and weld tape did not stick to the previous layer, i.e., frictional slip, the shear force would be fully decoupled from the build and no upward system resonance shift would occur. It is believed that when the welder sticks to the UAM build, the surface asperities of the foil at the interface undergo large amounts of plastic deformation through shear, which then promotes bonding. Others have also noted low amounts of frictional slip in 9 kW UAM when welding at higher loads (4–6 kN). Specifically, heat

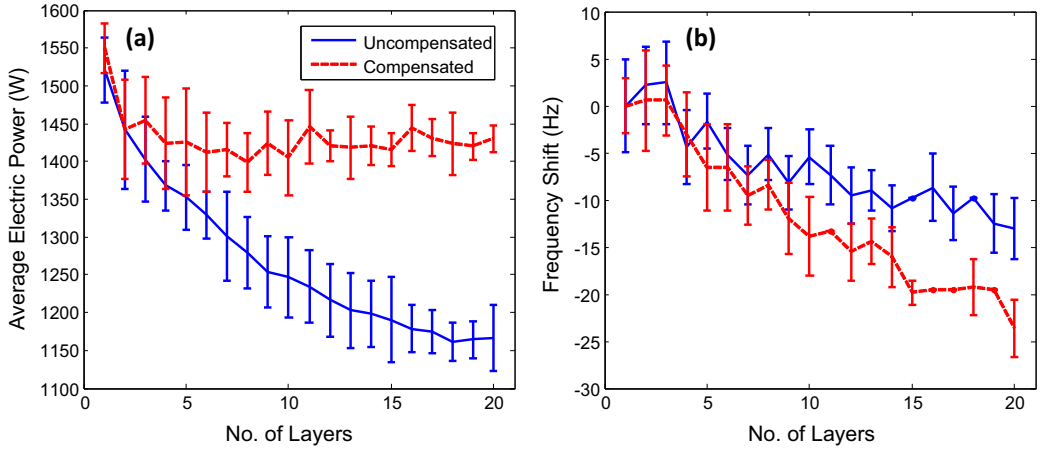

Fig. 19. Power and excitation frequency shift during UAM stack construction: (a) average electric weld power vs. number of layers; (b) excitation frequency shift vs. number of layers. The compensated power trace in (b) shows an increased amount of frequency shift.

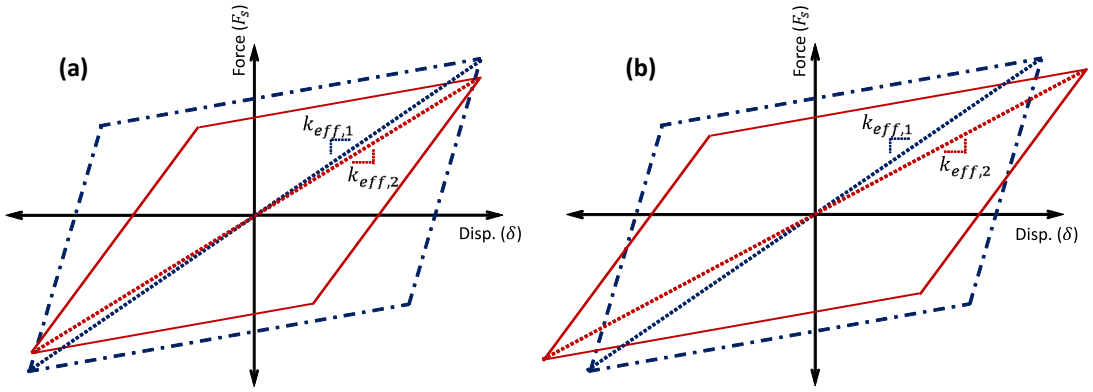

Fig. 20. Frequency shift mechanisms during UAM: (a) less plastic hardening decreases the effective build stiffness; (b) more plastic deformation decreases the effective build stiffness.

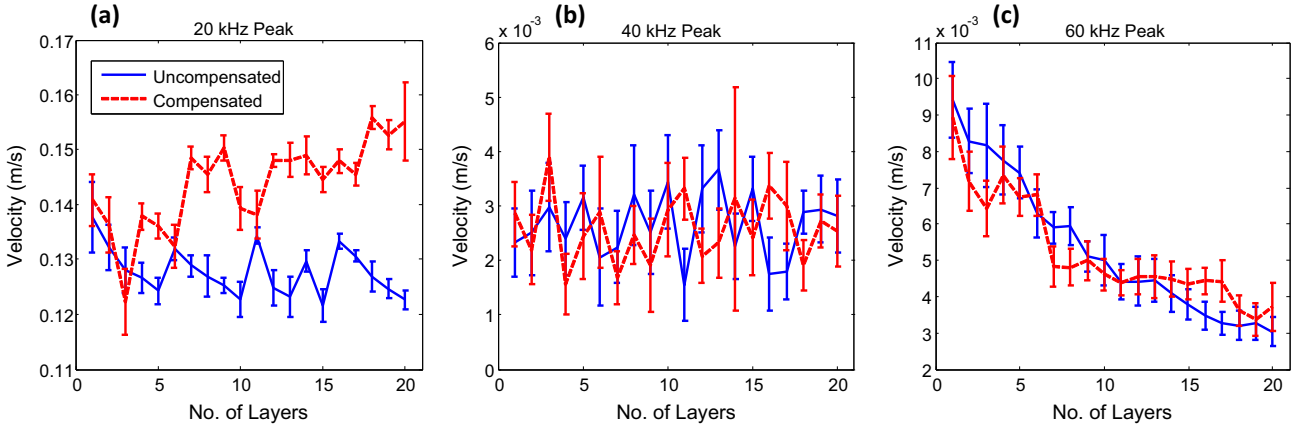

Fig. 21. Harmonic content during UAM stack construction for the approximate locations of 20, 40, and 60 kHz: (a) 1st harmonic, 20 kHz; (b) 2nd harmonic, 40 kHz; (c) 3rd harmonic, 60 kHz. The influence of power compensation increases the magnitude of the 1st harmonic, but does not influence the other harmonics. Due to the UAM build becoming more compliant with construction, the magnitude of the 3rd harmonic decreases. Harmonic content was found using FFT analysis using a Hamming processing window, a block size of 81,920 (6.5 Hz resolution), and by averaging the harmonic peak value with three points below and above it, i.e., seven total points total used to estimate content around the peak. Seven points were used for averaging content because reliably and consistently estimating the peak harmonic response is difficult with the processing block resolution.

generation within the weld was found to correlate well with plastic deformation heating and not frictional slip [11]. Also, normal force was found to not be statistically significant on UAM weld strength [22]. This concept of stick producing good bonds through shear deformation is contrary to the work of others [26]. However, this prior work did not include plastic deformation of the weld tape as a bonding mechanism. Instead, the stick condition was assumed to purely limit interfacial sliding.

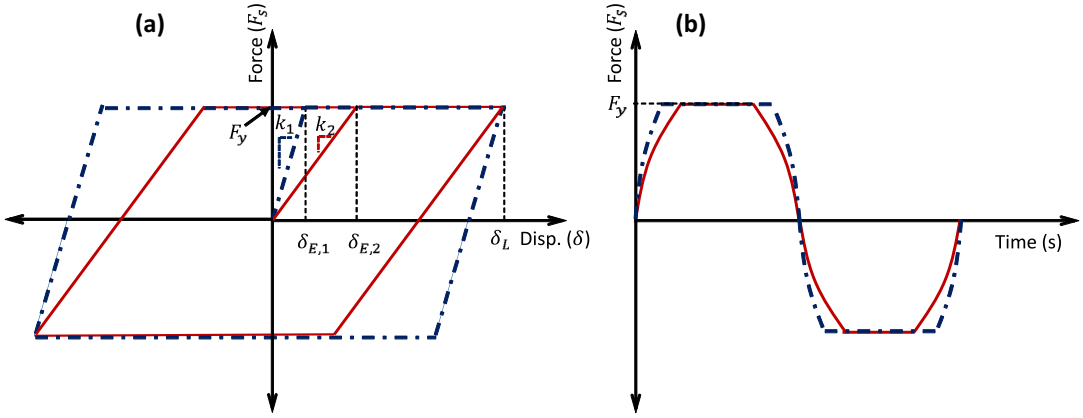

Fig. 22. Proposed shear force profile during welding using evidence from welder velocity frequency response measurements and H_m^*: (a) force-displacement; (b) force-time. Due to the UAM build becoming more compliant with more layers, the behavior of the forcing function becomes less square like with more layers.

The 10% decrease in velocity during welding (see Fig. 3(a)) occurs because (i) the motional feedback method employed by the ultrasonic generator may exhibit error when tracking the amplitude and (ii) the sonotrode deforms slightly during welding operations. To explore the motional feeback error, the presented LTI model can be used by evaluating the difference in welder velocity between two different welding states, i.e., welding and not welding. Because voltage is held constant between these two welding states, the voltage difference between the two states is zero. Consequently, with the use of (5) it can then be found that the difference in electric current is proportional to the difference in shear force,

$$H_e^* \Delta i = H_{em}^* \Delta F_s. \tag{20}$$

It is assumed in expression (20) that FRF magnitude is the same when welding or not welding and that system energy is predominately concentrated at the excitation frequency (ω_o). FRF magnitude dependence on welding will be discussed in the next section. Eq. (20) can then be used to explain the difference in welder velocity by relating it to the difference in shear force,

$$\Delta \dot{\delta} = \left(\frac{H_{em}^{*2}}{H_e^*} - H_m^* \right) \Delta F_s. \tag{21}$$

Eq. (21) demonstrates that shear force can influence welder velocity if the FRF term is not zero. Ideally, this FRF term equates to zero if motional feedback completely removes the electrical impedance influence of the transducer, see (6). However, if the electrical impedance of the transducer is not completely removed, the FRF term will not equate to zero and welder velocity will not be held constant when welding. The influence of remaining transducer impedance on welder performance was discussed earlier in Section 6 when evaluating the influence of normal force on welder effort.

To investigate the influence of sonotrode deformation on welder amplitude, a reduced fidelity linear elastic solid model of the sonotrode was analyzed in COMSOL Multiphysics. The goal of this simulation is not to fully describe the deformation behavior of the sonotrode, but to gain insight into the magnitude and behavior of the deformation. The built-in High-Strength Alloy Steel material option within COMSOL was used as the material in the model while the contact width for the force was chosen to be 0.5 cm from experimental observations. The mesh of the model utilized the physics controlled fine option within COMSOL. The reduced fidelity model along with boundary conditions for the simulation are shown in Fig. 23(a). Because the sonotrode is constrained against the weld surface of the build with a prescribed normal force, a deformation constraint was placed on the tool piece. The simulation output for a 9.65 cm diameter tool piece with an applied 2000 N distributed load is shown in Fig. 23(b). A 2000 N load was used because this is near the shear force estimate found in Section 5. Because the sonotrode is designed to operate in the longitudinal mode of vibration near 20 kHz, the static assumption is valid due to the self-exciting deformation modes of the sonotrode being sufficiently far away [36].

It is shown in Fig. 23(b) that the maximum deformation of the tool is near 1.5 μm. This deformation magnitude is similar to the velocity decrease of 0.25 m/s in Fig. 3(a). This velocity decrease correlates to an amplitude magnitude estimate of near 2 μm. This estimate was found by dividing the velocity decrease by frequency in rad/s, i.e., harmonic excitation assumption. In practice, obtaining the maximum deformation of the tool piece is not feasible because the laser vibrometer cannot reliably focus on the very tip of the tool piece. Nonetheless, this analysis shows that sonotrode deformation is likely a contributing factor to the decreased amplitude during welding and may be a larger contributor at higher shear force loads.

8.2. Influence of UAM build dynamics

The influence of UAM build dynamics on system dynamics can be studied by replacing welder shear force in Fig. 5(b) with a prescribed forcing function or a load impedance function (Z_{LD}) to describe energy transfer into the weld for UAM components. To describe UAM build dynamics in a general way for an Al 6061 stack, a complex stiffness [42] load impedance can be used,

$$Z_{LD} = \frac{k_{eff}}{j\omega}(1 + j\eta), \tag{22}$$

where k_{eff} is the effective stiffness of the UAM build and η is the loss factor or energy transfer efficiency of the process. This complex stiffness expression describes UAM build stiffness and damping, independent of frequency. In other words, a hysteretic damping model was chosen to model system losses because plastic deformation character would show little change near the excitation frequency when the PLL controller moves the excitation frequency. Damping from plastic deformation is typically described with a Coulomb-friction model [42], like bilinear hysteresis [43,44]. The purpose of the presented impedance function is not to describe the elasto-plastic interaction during UAM but to describe the UAM build dynamics in a general way.

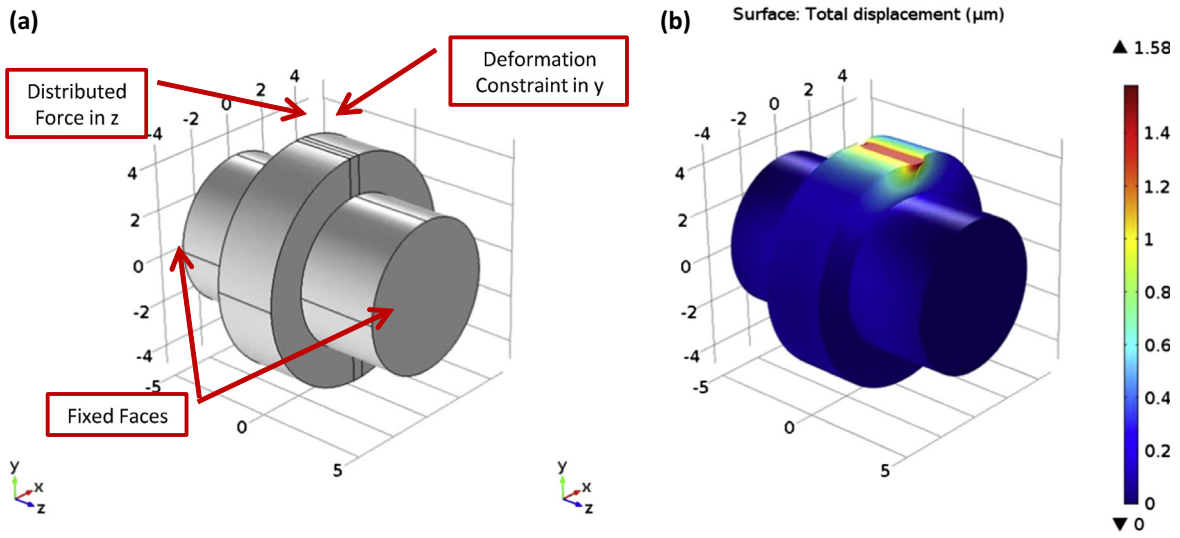

Fig. 23. Sonotrode deformation analysis from shear loading: (a) reduced model of sonotrode tool piece with assumptions; (b) deformation contour of 9.65 cm diameter tool piece with applied 2000 N distributed load.

To describe the influence of the UAM build onto the system, the load impedance was implemented by introducing effective build stiffness without damping initially ($\eta = 0$) and then introducing a loss factor ($\eta = 0.25$). To estimate the effective build stiffness, system stiffness was increased until a 75 Hz frequency shift was accomplished, see $\eta = 0$ traces in Figs. 24 and 25. This 75 Hz frequency shift was chosen because it was observed when welding an Al 6061 stack, see Fig. 3(b). The required build stiffness to cause this frequency shift is less than 1% of the assembly stiffness. Also, because energy is being stored in the system, no change in system response magnitude occurs. Because the welder is capable of moving the excitation frequency during welding, it can be inferred that FRF response will not change due to this added stiffness. For illustration purposes, a loss factor of 0.25 or a damping capacity of 25% was chosen to show the behavior of system losses during UAM due to large amounts of plastic deformation occurring. The $\eta = 0.25$ curves in Figs. 24 and 25 illustrate that the system response decreases due to energy no longer being stored within the welding assembly and being transferred to the weld interface. A summary of key lumped parameter estimates for this analysis are shown in Table 9.

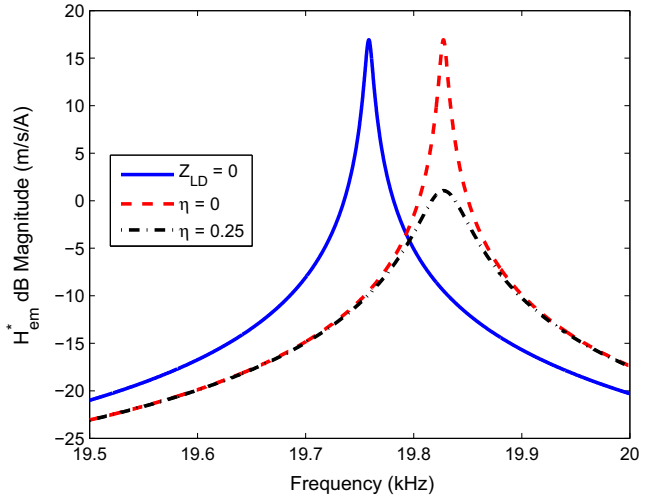

Fig. 24. Estimation of UAM build stiffness via a 75 Hz frequency shift and the investigation of UAM build stiffness on FRF magnitude. Due to stiffness not influencing FRF magnitude, FRF magnitude would be consistent when system resonance changes under load. Damping or energy leaving the system is shown to decrease system response.

9. Concluding remarks

A linear time invariant (LTI) model of the UAM process has been proposed to describe process dynamics by explicitly specifying welder shear force as a system input. To verify and to identify LTI model parameters, equivalent circuit analysis, empirical FRF estimation, and characterization measurements, were utilized. These characterization techniques and models can be applied to state-of-the-art UAM systems, can be used to improve controller design, and to ensure welder consistency across various welder assemblies. Welder consistency is of utmost importance as the use of UAM continues to expand.

Welder shear force and welder efficiency were estimated for the first time in UAM using this LTI model. Shear force magnitude and efficiency estimates were found to be near 2000 N and 80%, respectively. The influence of welder amplitude, normal force, and weld speed on shear force magnitude and welder efficiency was also evaluated. Normal force and weld speed show little to no influence while welder amplitude showed significant influence. The strong influence of welder amplitude occurs because of differences in elastic and plastic compliance between amplitude levels. The LTI model, experimental FRF measurements, and high frequency in-situ velocity measurements of the welder were also used to improve understanding of harmonic content and frequency shift behaviors in UAM. From this harmonic content behavior, shear force character can be estimated and understood as UAM build compliance changes.

An upward frequency shift on the order of 75 Hz occurs when welding Al 6061 because the UAM build stiffens the overall system. System stiffening can only occur if the sonotrode sticks to the UAM build. Otherwise, no system coupling would occur and no frequency shift would be observed. Using a lumped parameter model of the welding assembly and the observed 75 Hz resonant frequency shift, the effective build stiffness was found, which is less than 1% of the assembly stiffness.

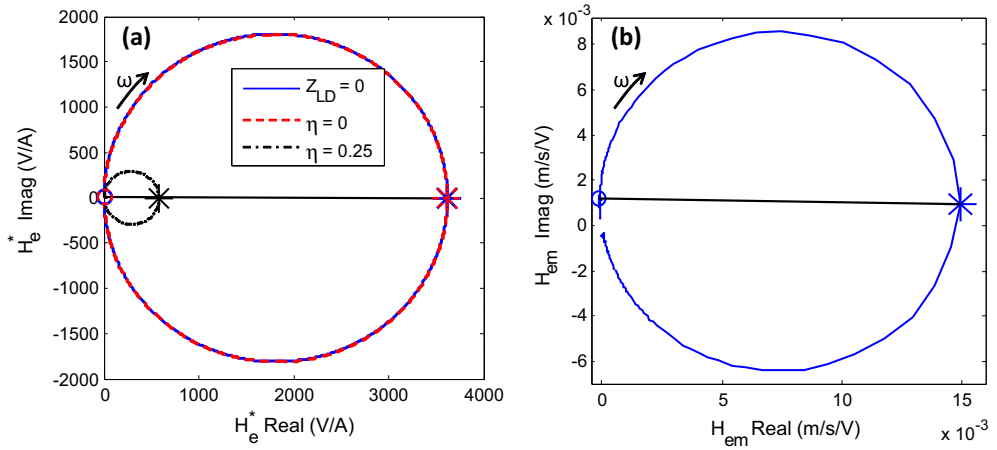

Fig. 25. Nyquist plots: (a) estimated motional impedance locus, H_e^*; (b) measured admittance locus, H_{em}. Resonant frequencies for each locus are marked with an asterisk while adjacent locus points are marked with circles. Loading the system without damping does not change the motional impedance locus due to the diameter remaining constant. The decrease in locus diameter occurs only when damping is introduced [34]. The resonant frequency location in the motional impedance locus occurs at 0 degrees because the electro-mechanical coupling coefficient is assumed to be real valued [34]. To verify this assumption, the H_{em} admittance locus is plotted. The resonant peak has a phase location < 1 degrees, which supports the real valued coupling coefficient assumption of 0 degrees.

Table 9
Key lumped parameter values used to describe UAM stack dynamics. Effective build stiffness (k_{eff}) was chosen by increasing the system resonance 75 Hz. A high loss factor (η) was chosen to illustrate the influence of the large amount of plastic deformation on system response during UAM.

Model variable	Value
K_t (GN/m)	30.49
k_{eff} (GN/m)	0.02
η	0.25

Acknowledgments

This material is based upon work supported by the National Science Foundation, CMMI Division Grant No. 1538275. Support for A.H. comes from a NSF Graduate Fellowship under Grant No. 1102690 and from the member organizations of the Smart Vehicle Concepts Center (http://www.SmartVehicleCenter.org), a National Science Foundation Industry/University Cooperative Research Center. Any opinions, findings, and conclusions or recommendations expressed in this material are those of the authors and do not necessarily reflect the views of the National Science Foundation. The authors would like to thank I.V. Adamovich and B. Goldberg of OSU's Non-Equilibrium Thermodynamics Laboratory for helping with the high voltage measurements of the welder.

References

[1] D. White, Ultrasonic consolidation of aluminum tooling, Adv. Mater. Process. 161 (1) (2003) 64–65.
[2] K. Graff, ASM Handbook: Volume 6A: Welding Fundamentals and Processes: Ultrasonic Additive Manufacturing, American Society for Metals International, 2011.
[3] K. Graff, M. Short, M. Norfolk, Very High Power Ultrasonic Additive Manufacturing (VHP UAM), in: International Solid Freeform Fabrication Symposium, Austin, TX, 2011.
[4] E. Neppiras, Ultrasonic welding of metals, Ultrasonics 3 (3) (1965).
[5] H. Daniels, Ultrasonic welding, Ultrasonics 3 (4) (1965).
[6] K. Graff, AWS Handbook 9th Edition: Volume3: Ultrasonic Welding of Metals, American Welding Society, 2001.
[7] K. Johnson, Interlaminar Subgrain Refinement in Ultrasonic Consolidation, Ph. D. thesis, Loughborough University, Loughborough, UK, 2008.
[8] R. Dehoff, S. Babu, Characterization of interfacial microstructures in 3003 aluminum alloy blocks fabricated by ultrasonic additive manufacturing, Acta Mater. (2010) 1–12.
[9] M. Sriraman, S. Babu, M. Short, Bonding characteristics during very high power ultrasonic additive manufacturing copper, Scripta Mater. 62 (2010) 560–563.
[10] H. Fujii, M. Sriraman, S. Babu, Quantitative evaluation of bulk and interface microstructures in Al-3003 alloy builds made by very high power ultrasonic additive manufacturing, Metall. Mater. Trans. A: Phys. Metall. Mater. Sci. 42 (13) (2011) 4045–4055.
[11] M. Sriraman, M. Gonser, H. Fujii, S. Babu, M. Bloss, Thermal transients during processing of materials by very high power ultrasonic additive manufacturing, J. Mater. Process. Technol. 211 (2011) 1650–1657.
[12] G. Janaki Ram, C. Robinson, Y. Yang, B. Stucker, Use of ultrasonic consolidation for fabrication of multi-material structures, Rapid Prototyp. J. 13 (4) (2007) 226–235.
[13] J. Obielodan, A. Ceylan, L. Murr, B. Stucker, Multi-material bonding in ultrasonic consolidation, Rapid Prototyp. J. 13 (3) (2010) 180–188.
[14] C. Hopkins, S. Fernandez, M. Dapino, Statistical characterization of ultrasonic additive manufacturing Ti/Al composites, J. Eng. Mater. Technol. 132 (2010).
[15] A. Truog, Bond Improvement of Al/Cu Joints Created by Very High Power Ultrasonic Additive Manufacturing, Master's thesis, The Ohio State University, Columbus, OH, 2012.
[16] J.M. Sietins, Exploring Diffusion of Ultrasonically Consolidated Aluminum and Copper Films Through Scanning and Transmission Electron Microscopy, Ph.D. thesis, University of Delaware, Newark, DE, USA, 2014.
[17] C. Kong, R. Soar, P. Dickens, Ultrasonic consolidation for embedding SMA fibres within aluminium matrices, Compos. Struct. 66 (2004) 421–427.
[18] C. Kong, R. Soar, Method for embedding optical fibers in an aluminum matrix by ultrasonic consolidation, Appl. Opt. 44 (30) (2005) 6325–6333.
[19] E. Siggard, Investigative Research into the Structural Embedding of Electrical and Mechanical Systems Using Ultrasonic Consolidation, Master's thesis, Utah State University, Logan, UT, 2007.
[20] X. Cheng, A. Datta, H. Choi, X. Zhang, X. Li, Study on embedding and integration of microsensors into metal structures for manufacturing applications, J. Manuf. Sci. Eng. 129 (2007) 416–424.
[21] R. Hahnlen, Characterization and Modeling of Active Metal-Matrix Composites with Embedded Shape Memory Alloys, Ph.D. thesis, The Ohio State University, Columbus, OH, 2012.
[22] P. Wolcott, A. Hehr, M. Dapino, Optimized welding parameters for Al 6061 ultrasonic additive manufactured structures, J. Mater. Res. 29 (17) (2014).
[23] C. van der Burgt, H. Pijls, Motional positive feedback systems for ultrasonic power generators, IEEE Trans. Ultrason. Eng. 10 (1) (1963).
[24] B. Richter, J. Twiefel, J. Wallaschek, Energy Harvesting Technologies: Ch4: Piezoelectric Equivalent Circuit Models, Springer, 2009.
[25] J.M. Gibert, E.M. Austin, G. Fadel, Effect of height to width ratio on the dynamics of ultrasonic consolidation, Rapid Prototyp. J. 16 (4) (2010).
[26] J.M. Gibert, G. Fadel, M.E. Daqaq, On the stick-slip dynamics in ultrasonic additive manufacturing, J. Sound Vib. 332 (2013) 4680–4695.
[27] C. Robinson, C. Zhang, G. Janaki-Ram, E. Siggard, B. Stucker, L. Li, Maximum height to width ratio of free-standing structures built by ultrasonic consolidation, in: Proceedings of the 17th Solid Freeform Fabrication Symposium, Austin, TX, 2006.
[28] A. Hehr, P.J. Wolcott, M.J. Dapino, Effect of weld power and build compliance on ultrasonic consolidation, Rapid Prototyp. J. 22 (2) (2016).
[29] J.M. Gibert, Dynamics of Ultrasonic Consolidation, Ph.D. thesis, Clemson University, Clemson, SC, USA, 2009.
[30] K. Graff, Power Ultrasonics: Ch6: Power Ultrasonic Transducers: Principles and Design, Elsevier, 2015.
[31] E. Neppiras, New magnetostrictive materials and transducers: Part I, J. Sound Vib. 8 (3) (1968).

[32] E.A. Neppiras, Motional feed-back systems for ultrasonic transducers, in: Ultrasonics, London, UK, 1971.
[33] Dukane Communication, Private Communication, 2015.
[34] F. Hunt, Electroacoustics: The Analysis of Transduction and Its Historical Background, Harvard University Press, Cambridge, 1954.
[35] W.P. Mason, Electromechanical Transducers and Wave Filters, D. Van Nostrand Company, Inc., 1942.
[36] A.J. Hehr, Process Control and Development for Ultrasonic Additive Manufacturing with Embedded Fibers, Ph.D. thesis, The Ohio State University, Columbus, OH, USA, 2016.
[37] IEEEI, IEEE Std 176-1987: Standard on Piezoelectricity, 1988.
[38] AE Techron, Technical Manual: LVC5050 Power Supply Amplifier, 2002.
[39] E. De Vries, Mechanics and Mechanisms of Ultrasonic Metal Welding, Ph.D. thesis, The Ohio State University, Columbus, OH, 2004.
[40] R. Friel, Power Ultrasonics: Ch13: Power Ultrasonics for Additive Manufacturing and Consolidation of Materials, Elsevier, 2015.
[41] F. Balle, G. Wagner, D. Eifler, Characterization of the Ultrasonic Welding Process through High-resolution Laser-Doppler Vibrometry, Polytec InFocus Magazine 1.
[42] C. de Silva, Vibration: Fundamentals and Practice, CRC Press LLC, 2000.
[43] T.K. Caughey, Sinusoidal excitation of a system with bilinear hysteresis, J. Appl. Mech. 27 (4) (1960).
[44] W. Iwan, A distributed-element model for hysteresis and its steady-state dynamic response, J. Appl. Mech. 33 (4) (1966).